Biosensors and Bioelectronics: X 21 (2024) 100552

Contents lists available at ScienceDirect

Biosensors and Bioelectronics: X

journal homepage: www.journals.elsevier.com/biosensors-and-bioelectronics-x

Intact photosynthetic bacteria-based electrodes for self-powered metal ions monitoring

Jefferson Honorio Franco [a], Paolo Stufano [b], Rossella Labarile [a,c], Dario Lacalamita [a], Pierluigi Lasala [a,c], Elisabetta Fanizza [a,c], Massimo Trotta [c], Gianluca Maria Farinola [a], Matteo Grattieri [a,c,*]

[a] Dipartimento di Chimica, Università Degli Studi di Bari "Aldo Moro", Via E. Orabona 4, Bari, 70125, Italy
[b] CNR-NANOTEC, Consiglio Nazionale Delle Ricerche, Bari, 70125, Italy
[c] IPCF-CNR Istituto per I Processi Chimico Fisici, Consiglio Nazionale Delle Ricerche, Via E. Orabona 4, Bari, 70125, Italy

ARTICLE INFO

Keywords:
Photobioelectrochemistry
Photo-induced extracellular electron transfer
Metal ions
Biophotoanode
Purple bacteria
Redox polymers
Biosensors

ABSTRACT

The low-cost and early monitoring of metal ion contaminants is paramount to prevent widespread contamination of water environments. Self-powered microbial electrochemical sensors represent an interesting approach to achieving this goal. Purple non-sulfur bacteria have a versatile metabolism and a well-characterized photosynthetic system, making them an ideal candidate for developing biohybrid technologies. In this work, we report the use of these bacteria in biophotoelectrodes to develop self-powered monitoring systems for two common pollutants, $NiCl_2$ and $CuSO_4$. The microbial biophotoelectrode was obtained on a homemade poly-hydroxybutyrate-carbon nanofibers electrode modified with a redox-adhesive polydopamine matrix-based entrapping the purple bacterium *Rhodobacter capsulatus*. The presence of 500 μM $NiCl_2$ resulted in a 60 % decrease in current density, while the simultaneous presence of 100 μM $NiCl_2$ and 100 mM $CuSO_4$ led to an 83 % current inhibition. Given the implementation of the biophotoelectrode in the field, the biohybrid system was tested in a complex matrix containing beer, demonstrating the promising ability of the photoelectrochemical system to act as an efficient biosensor in complex solutions. Finally, the biohybrid electrode was coupled to a cathode performing oxygen reduction, which allowed obtaining a self-powered monitoring system, paving the way for the future implementation of a low-cost monitoring system for widespread metal ions contaminant monitoring.

1. Introduction

Microbial electrochemical systems have garnered significant attention in the last decades due to the various technological possibilities enabled by the coupling of self-replicating biological catalysts and abiotic electrodes (Fan et al., 2021(Bedendi et al., 2022)). Recently, several studies have reported using photosynthetic entities as biocatalysts (Operamolla et al., 2015; Zhang and Tremblay, 2017; Zhu et al., 2023). Among the photosynthetic entities, the use of intact bacterial cells attracted particular interest thanks to their versatile metabolism that allows using various organic compounds as substrates and their efficiency in converting sunlight energy to photoexcited electrons (Operamolla et al., 2015). Specifically, *Rhodobacter capsulatus* (*R. capsulatus*) is a purple non-sulfur photosynthetic bacterium (PNSB) that presents excellent metabolic versatility by utilizing organic compounds such as malic and succinic acid as substrates. Furthermore, *R. capsulatus* can act under diverse environmental conditions, allowing its efficient application as a biophotocatalyst (Giraud and Verméglio, 2008; Torquato and Grattieri, 2022; Beaver et al., 2022). Nevertheless, a recurrent hindrance when using intact PNSB systems for biophotoelectrode development is that the photosynthetic apparatus is deeply buried in the bacterial cell membrane, which acts as an insulating material, hindering the process of photoinduced electron transfer (PEET) from the photosynthetic apparatus to the electrode surface (Pankratova and Gorton, 2017; Kumar et al., 2017; Grattieri, 2020).

To address this issue, various artificial approaches were reported to tune extracellular electron transfer including the use of exogenous redox mediators, which provide the electrical wiring necessary to transport the electrons during the PEET process (Longatte et al., 2018; Sayegh et al., 2021). However, applying diffusible mediators is not preferable due to

* Corresponding author. Dipartimento di Chimica, Università Degli Studi di Bari "Aldo Moro", Via E. Orabona 4, Bari, 70125, Italy.
E-mail address: matteo.grattieri@uniba.it (M. Grattieri).

https://doi.org/10.1016/j.biosx.2024.100552
Received 14 June 2024; Received in revised form 16 September 2024; Accepted 7 October 2024
Available online 10 October 2024

their toxicity and unwanted release into the environment, leading to the search for more efficient alternatives (Longatte et al., 2018; Grattieri et al., 2019). Given the challenges associated with the transfer of electrons between the photosynthetic apparatus and the electrode surface, various approaches have been studied to facilitate this process (Hasan et al., 2014; Grattieri et al., 2020a, 2020b; Beaver et al., 2023). Notably, the unique features of a catecholamine neurotransmitter, dopamine, which provides a flexible surface coating like a redox adhesive matrix in its polymerized form, polydopamine (PDA), have been recently explored (Ding et al., 2016; Yun et al., 2022). A recent study from our group demonstrated the 5-fold enhancement of photocurrent production through entrapment of active purple bacteria cells on the electrode surface in a PDA matrix (Buscemi et al., 2022). Such an increase in photocurrent could be achieved thanks to both the redox mediation of the PDA matrix and its capability to enhance the local concentration of endogenous redox mediators (i.e., quinones and flavins) (Liu et al., 2019; Buscemi et al., 2022).

Another important aspect is the choice of electrode material to be utilized in the microbial electrochemical system, to ensure stability, biocompatibility, and high microbial colonization. Among various materials, transition metal oxides could be of interest for their stability and high surface area (Ahmad et al., 2023a; Ahmad et al., 2024). Carbon-based electrodes represent another class of interesting materials for microbial electrochemical systems (Santoro et al., 2017; Ahmad et al., 2023b). Recently, our group reported using homemade, low-cost, porous biobased electrodes with poly-3-hydroxypolybutyrate (PHB)-carbon nanofibers (CF) electrodes to enhance bacteria-electrode interaction and current production (de Moura Torquato et al., 2024). CF has very attractive features such as large surface area, chemical/thermal stability, and low cost, which provide an efficient electrode that combines desired surface and structural properties (Niu et al., 2011; Yadav et al., 2020).

The high sensing potential of microbial electrochemical systems has been reported in recent years, with interesting results enabled by the microbial ability to self-replicate and enhance signals through metabolic cascades and complex metabolisms (Prévoteau and Rabaey, 2017). Electrochemical biosensors based on intact bacterial cells do not require enzyme isolation and purification, making them more cost-effective and easier to apply (ElMekawy et al., 2018; Cui et al., 2019). Recent studies have shown the use of microbial fuel cell (MFC)-based biosensors to obtain self-powered devices for the detection and monitoring of metal pollutants in wastewater (Yu et al., 2017; Grattieri and Minteer, 2018; Dai et al., 2019). In addition to wastewater (Kamali et al., 2023), these devices could find application in monitoring effluents from petroleum and metal industries (Hemdan et al., 2022; Kondaveeti et al., 2023). Among different metal ions generated by various industrial activities, nickel (Ni) is considered a widespread environmental pollutant (Das et al., 2019). Ni represents a micronutrient crucial for human health by stimulating hormonal activity (Zdrojewicz et al., 2016). However, prolonged exposure to higher doses of Ni through food or water intake can cause serious side effects on human health (Das et al., 2019; Genchi et al., 2020). MFC biosensors have been developed with the aim of detecting and monitoring the presence of nickel ions in industrial effluents (Anchidin-Norocel et al., 2021) by potentiometric transduction (Verma and Singh, 2006), electrochemical (Rezaei and Rezaei, 2006; Nurak et al., 2013) and spectrophotometric techniques. An electrochemical biosensor based on enzyme inhibition was developed utilizing *Bacillus sphaericus* MTCC 5100 to produce urease. This enzyme catalyzes the hydrolysis of urea into NH_4^+ and its activity is inhibited by Ni^{2+}. The system allowed biosensing in industrial effluents of an electroplating unit with a range of Ni^{2+} detection of 0.03–0.68 nM (Verma and Singh, 2006). Tibazarwa et al. (2001) constructed a biosensor containing *Ralstonia eutuopha* strain AE2515 for the detection of Ni^{2+} in soil samples. The bioluminescence response achieved a linearly correlated Ni^{2+} with the range 0.1–60 μM, confirming the highly selective AE2515 biosensor strain for nickel (Tibazarwa et al., 2001).

The electrical wiring of intact biological catalysts to electrodes allows obtaining simpler electrochemical biosensing systems (Grattieri et al., 2020; Simoska et al., 2021), however, no previous studies discussed hybrid microbial electrochemical systems using photosynthetic bacteria to obtain self-powered biosensors for monitoring of metal ions in complex solutions.

Herein, we target the development of a bio-based, self-powered, and low-cost monitoring system, where the biohybrid electrochemical device produces a power output that can directly correlate to a target contaminant's concentration. For this purpose, we report the design of a biophotoelectrode containing *R. capsulatus* electropolymerized with PDA onto bacterial-PHB-CF electrodes. Electrochemical and spectroscopic techniques assessed the performance and stability of the bacteria-based photoelectrodes in the presence and absence of light. The effects of different concentrations of nickel chloride ($NiCl_2$) and copper sulfate ($CuSO_4$) are discussed, both during the system's operation in a classic three-electrode setup and in self-powered mode. The catalytic performance of the hybrid system was also evaluated in a complex matrix such as a commercial beer. The latter mode of operation opens the door to developing portable devices performing sun-light driven on-demand metal ions monitoring.

2. Experimental

2.1. Chemicals

Malic acid, magnesium chloride ($MgCl_2$), and 3-(N-Morpholino) propanesulfonic acid (MOPS) were purchased from Sigma-Aldrich. Dopamine hydrochloride (MW = 189.64 uma, CAS 62-31-7), $NiCl_2$, and $CuSO_4$ were purchased from Sigma Aldrich. All the solutions were prepared by dissolving the appropriate amounts of the salts in Ultrapure Milli-Q water (18 MΩ cm^{-1}). All chemicals were used as received without further purification.

2.2. Bacteria growth

R. capsulatus strain DSMZ 152 was obtained from the German Collection of Microorganisms and Cell Cultures (DSMZ) and grown in a liquid growth medium at 10 % *v/v* in sterile 50 mL bottles sealed with airtight stoppers. The growth medium contained malic acid (4.0 g L^{-1}), $(NH_4)_2SO_4$ (1.0 g L^{-1}), $CaCl_2 \cdot 2H_2O$ (75 mg L^{-1}), $MgSO_4 \cdot 7H_2O$ (200 mg L^{-1}), $FeSO_4 \cdot 7H_2O$ (12 mg L^{-1}), EDTA (20 mg L^{-1}), thiamine (1 mg L^{-1}), biotin (15 mg L^{-1}), K_2HPO_4 (0.9 g L^{-1}), KH_2PO_4 (0.6 g L^{-1}), and a trace elements solution (1.0 mL L^{-1}) prepared as previously reported (Grattieri et al., 2019). Before sterilization of the culture medium at 125 °C for 25 min (Systec VX55), the pH was adjusted to 6.8 using 5 M NaOH. After sterilization, the trace elements, $MgSO_4$, $CaCl_2$, $FeSO_4$, and biotin were filtered through a 0.20 μm filter (Puradisc 25) and added to the culture medium. Bacterial growth was carried out in an incubator (IKA KS 3000 I control) at 28 °C under constant illumination provided by an 80 W incandescent lamp.

2.3. Polyhydroxybutyrate - carbon nanofibers (PHB - CF) electrode preparation

The PHB-CF electrode was prepared via the casting process following the procedure reported by (de Moura Torquato et al., 2024). First, 360 mg of polyhydroxybutyrate (PHB) and 240 mg of carbon nanofibers (CF) (ratio 3:2) were weighed and mixed in 20 mL of dichloromethane (CH_2Cl_2). The suspension obtained was heated to 100 °C and stirred at 700 rpm (Velp Scientifica Are magnetic heating stirrer) for 1 h. The casted solution was then placed in a Petri dish to evaporate the solvent. The final composite material was cut into slices measuring 1.5 × 0.5 cm and washed with ethanol to remove the impurities. After that, the aerobic polymerization was performed by complete dip of the electrodes in a 5 mM dopamine solution in MOPS buffer (pH 8) for 1 h. Finally, the

electrodes underwent heat treatment at 170 °C for 1 h and stored at room temperature until use.

2.4. Biohybrid electrodes preparation

The biohybrid electrodes were prepared following the procedure previously reported by our group (Buscemi et al., 2022). Briefly, after 72 h of bacterial growth under constant illumination, *R. capsulatus* cells were collected and centrifuged in two steps: (i) centrifugation at 5700 rpm for 20 min at 20 °C (MPW Med. Instruments-260 R), and (ii) the cells were resuspended in 1 mL of the electrolyte pH 7 (containing 20 mM MOPS buffer + 10 mM $MgCl_2$ + 50 mM malic acid) and further centrifugation at 10 000 rpm for 10 min (Giorgio Bormac S.r.l. Multispin 12). At the same time, a 10 mM dopamine solution was prepared and dissolved in a buffer at pH 8 (containing 20 mM MOPS buffer + 10 mM $MgCl_2$). After the second centrifugation, the bacterial suspension was prepared at 2 g mL^{-1} in 10 mM buffer pH 8.0. Subsequently, the bacterial suspension was transferred to a 2 mL Eppendorf in a 1:1 ratio with the dopamine solution (final concentration of bacteria 1 g mL^{-1}). The solution was stirred at 500 rpm (Metrohm 728 Magnetic Stirrer) for 1 h under aerobic conditions to start the chemical polymerization of the dopamine monomer (Buscemi et al., 2022; Alfieri et al., 2018).

To cover an electrode surface area of 0.5 cm^2, 50 μL of the polymerized solution (50 mg of bacterial cells entrapped in the polymeric matrix) was pipetted directly onto the PHB-CF electrode (de Moura Torquato et al., 2024) and left to dry for 1 h before performing the electrochemical polymerization step. If the bacterial cells entrapped in the PDA matrix are left to dry on the electrode surface for times longer than 2 h a loss of bioelectrocatalytic performance was obtained. Accordingly, if the bioelectrode is not required for immediate use, the entrapped bacterial cells should be stored at 4 °C until use (up to two days). The electrochemical polymerization is performed through repeated cyclic voltammetry (20 cycles) in a potential window of - 0.13 V–0.52 V *vs* Ag|AgCl (3 M NaCl) at a scan rate of 20 mV s^{-1}.

2.5. Morphological characterization

Dehydrated samples of the biohybrid electrode were prepared using subsequent 25%, 50%, 75%, 95%, and 100% ethanol solutions. The samples were mounted on a stainless-steel sample holder and gold sputtered before analysis. Scanning Electron Microscopy (SEM) analysis was performed with a Zeiss-Sigma Field Emission-Scanning electron microscope (Carl Zeiss Co., Oberkochen, Germany) operating at 5 kV and equipped with an in-lens secondary electron detector and an INCA Energy Dispersive Spectroscopy (EDS) detector.

2.6. Electrochemical experiments

All the electrochemical experiments were performed in triplicates at room temperature using a PalmSens4 potentiostat equipped with a three-electrode electrochemical cell.

A platinum wire was used as a counter electrode, Ag|AgCl (3 M NaCl) was the reference electrode, and the working electrode was the *R.caps*-PDA polymerized on the PHB-CF. Various control electrodes were also prepared, as described below. The photobioelectrocatalysis performance of *R. capsulatus* entrapped in the PDA matrix (*R.caps*-PDA) was investigated by cyclic voltammetry (CV) and chronoamperometry experiments. The utilized electrolyte for the electrochemical cell consisted of 30 mL of 50 mM malic acid, 10 mM $MgCl_2$, and 20 mM MOPS. To confirm the biotic origin of the photocurrent, control experiments were performed with PHB-CF in two configurations: (i) heat-treated *R. capsulatus* for 2 h at 120 °C (*R.caps*$_{HT}$-PDA), and (ii) an abiotic electrode coated with only PDA. The effects of $NiCl_2$ on the photobioelectrocatalytic activity of *R. caps*-PDA and *R.caps*$_{HT}$-PDA electrodes were studied under exposure to concentrations of $NiCl_2$ in a range of 100–500 μM. Before the photoelectrochemical analyses, Argon gas (Rivoira UN1006 compressed Argon 99% pure) was purged into the electrolyte solution for 20 min to remove oxygen and obtain a controlled anaerobic environment. CV and amperometric i-t tests were performed in the presence and absence of illumination, which was provided with a fiber optic lamp (Schott KL 1500 LCD) equipped with a 10 W bulb, generating an output light intensity of 150 mW cm^{-2} (measured with Gigahertz-Optik MSC15) to ensure light saturation.

The obtained biophotoelectrodes and control electrodes were characterized by CV performed at a scan rate of 5 mV s^{-1} in a potential window from −0.13 to 0.52 V (*vs* Ag/AgCl) at 25 ± 2 °C. The electrochemical performance of the CV's with the different bioelectrode configurations was evaluated by comparing the current density achieved for the second anodic scan at a potential of +0.32 V. This potential was selected to ensure a sufficient overpotential to drive the oxidation of the redox centers in the polydopamine matrix. Chronoamperometry experiments were performed at the potential of +0.32 V, switching the light/dark condition. Comparison of the amperometric performance of different PHB-based electrodes was evaluated based on average current densities under illumination. Concomitantly, the stability of the different working electrode configurations over time was evaluated by comparing the current density values at the end of the dark cycle.

Power density tests were performed to evaluate the performance of energy conversion of the photobioelectrochemical hybrid system operating as a self-powered biosensor. Accordingly, the developed biophotoelectrode was coupled to a Pt-cathode to obtain a complete photomicrobial fuel cell operating in a single-chamber setup (anode and cathode exposed to the same electrolyte, with no separator between them). The biophotoanode was used as both the counter and reference electrode, and the Pt cathode was used as the working electrode. Before performing a linear polarization on the cell, stabilization of the open-circuit potential (OCP) was allowed by recording the OCP for 10 min or until the value was stabilized.

Following stabilization, the OCP obtained was used as a starting value to perform the quasi-stationary linear sweep polarization at 0.2 mV s^{-2}, reaching a final potential of 0.01 V.

2.6.1. Bioelectrocatalysis assessment of the photosynthetic system performance in complex matrix

To investigate the possibility of employing the developed hybrid photocatalytic system for Ni ions monitoring in real samples, we characterized the electrochemical response of the hybrid electrode in an electrolyte containing a commercial beer with no further treatment before use. The same procedure described in the Experimental Section 2.5 was performed by adding beer to the electrolyte in a final concentration of 10 % (%v/v) and by stirring the solution for 15 min before starting the experiments. The electrochemical characterization was performed in the presence and absence of different concentrations of $NiCl_2$ to test the capability of the biosensor to operate using a complex matrix.

2.7. Spectrophotometric experiments

The evaluation of the photosynthetic apparatus of *R. capsulatus* cells was carried out by UV–Vis spectrophotometric measurements in the range 400–1000 nm using a Cary 5000 UV–Vis–NIR (Agilent Technologies) on samples containing *R. capsulatus* entrapped in the PDA matrix (*R.caps*-PDA), *R. capsulatus* without PDA (*R.caps*$_{WH}$-PDA), and heat-treated *R. capsulatus* (*R.caps*$_{HT}$-PDA). The *R.caps*-PDA and *R.caps*$_{WH}$PDA samples were also analyzed before and after exposure to 100, 200, and 500 μM $NiCl_2$ for 1 h. Samples of the bacteria cells were collected according to the centrifugation procedures described previously, proceeding with the aerobic polymerization for 1 h. All samples were incubated at room temperature for 1 h with different concentrations of $NiCl_2$. To evaluate possible damage to the photosynthetic apparatus of the bacterium after exposure to $NiCl_2$ and obtain high reliability of the results, the absorption spectra of *R.caps*-PDA and *R.*

caps$_{WH}$PDA were recorded immediately after sample preparation and after 1 h of incubation with different concentrations of $NiCl_2$. Therefore, based on the intensity of the absorbance band observed after this incubation period, the absorption spectra of cells exposed to $NiCl_2$ was compared with those of cells not exposed to the metal.

3. Results and discussion

3.1. SEM micrograph characterization

The SEM micrograph characterization of the biohybrid electrodes showed a dense distribution of PDA-embedded *R. capsulatus* bacterial cells over interconnected carbon fibers (Fig. 1A). At higher magnification (Fig. 1B), the homogeneous PDA matrix appeared as lumps over the *R. capsulatus* cells. The distribution of bacterial cells over the PHB-CF electrode and the swelling of the PDA matrix appeared unchanged prior (Fig. 1C) and after $NiCl_2$ exposure (Fig. 1D). Furthermore, the bacterial shapes exhibited no noticeable distinctions, suggesting that exposure to 500 μM of $NiCl_2$ did not affect bacterial morphology.

The EDS analysis confirmed the presence of $NiCl_2$ embedded into the PDA matrix (Fig. S1 A), which was not detected in control samples not exposed to $NiCl_2$ (Fig. S1 B). In addition, signals from C, O, Na, Mg, S, P, and Ca atoms were detected, due to the presence of bacterial cells and carbon nanofibers. The EDS micrographs of electrodes exposed to $NiCl_2$ (Fig. 2 A) showed the mapping distribution of the metal into the PDA matrix that embeds *R. capsulatus* bacterial cells (Fig. 2 B) as well as the distribution of C, O, Na, Mg, S, P, and Ca atoms (Fig. 2 C). The same atoms were also detected for the unexposed electrode used as control except for $NiCl_2$ and Ca (Fig. S2).

3.1.1. Effect of different concentrations of $NiCl_2$ on photobioelectrocatalysis

CV experiments were conducted to evaluate the photobioelectrocatalytic performance of the biohybrid electrodes. Fig. 3 displays the current density response for the photoelectrode and control electrodes (heat-treated (*R.caps*$_{HT}$-PDA) and only PDA-modified electrodes under anaerobic conditions in light and dark with different $NiCl_2$ concentrations.

Fig. 3 A and 3 B show the electrochemical response of the biohybrid *R.caps*-PDA electrode (black line), the control electrodes with heat-treated, *R.caps*$_{HT}$-PDA (red line), and with only PDA (blue line) in the light and dark, respectively. Under illumination, the hybrid system showed an increased current density (58 ± 3 μA cm^{-2}) at + 0.32 V compared to the control electrodes with the metabolically inactive bacteria or containing only PDA, corresponding to a 5-fold and 15-fold higher current density, respectively. In the dark, the hybrid system with active bacteria provided a 40 % lower current density compared to light conditions, confirming the capability of the photosynthetic apparatus to enhance energy conversion under illumination. The current density obtained in the dark for the control electrodes showed a similar trend compared to the results obtained in the light. The effect of increasing additions of $NiCl_2$, namely 100, 200, and 500 μM, was studied to evaluate the biocatalytic activity of the biohybrid system exposed to the contaminant (Fig. 3C and D). The addition of $NiCl_2$ in the range of 100–500 μM promoted the decrease of the current density in the light (Fig. 3 C) and dark (Fig. 3 D). Notably, the highest concentration added in the electrolyte (500 μM $NiCl_2$) resulted in significant inhibition (50 %) of the catalytic activity of *R.caps*-PDA with and without illumination. However, it is important to note that only for the CV performed under illumination it was possible to differentiate the current response obtained in the presence of various concentrations of $NiCl_2$. Conversely, in the dark, the current density obtained at + 0.32 V in the presence of 100 and 200 μM $NiCl_2$ was not significantly different. In addition, it should be noted that the current density of the *R.caps*$_{HT}$-PDA and the electrode containing only PDA did not change even when exposed to $NiCl_2$ (Figure S3, and Figure S4, respectively), proving that the variation in current results from the action of the pollutant on the metabolism of the bacterial cells.

3.1.2. Evaluation of the effect of $NiCl_2$ and $CuSO_4$ on photobioelectrocatalysis

To further investigate the possibility of utilizing the biohybrid electrode for metal ions monitoring, we tested the behavior of the hybrid system in the simultaneous presence of two metal ions. Fig. S5 displays the current density of the *R.cap*-PDA in the presence of both 100 μM $NiCl_2$ and 100 μM $CuSO_4$ in light and dark conditions. Under illumination (Fig. S5 A), the hybrid system in the presence of both metals showed a decreased catalytic activity (12 ± 0.5 μA cm^{-2}) compared to *R.caps*-PDA and *R.caps*-PDA + $NiCl_2$, providing 70 % and 55 % lower current density, respectively. The comparison of the CVs obtained in the

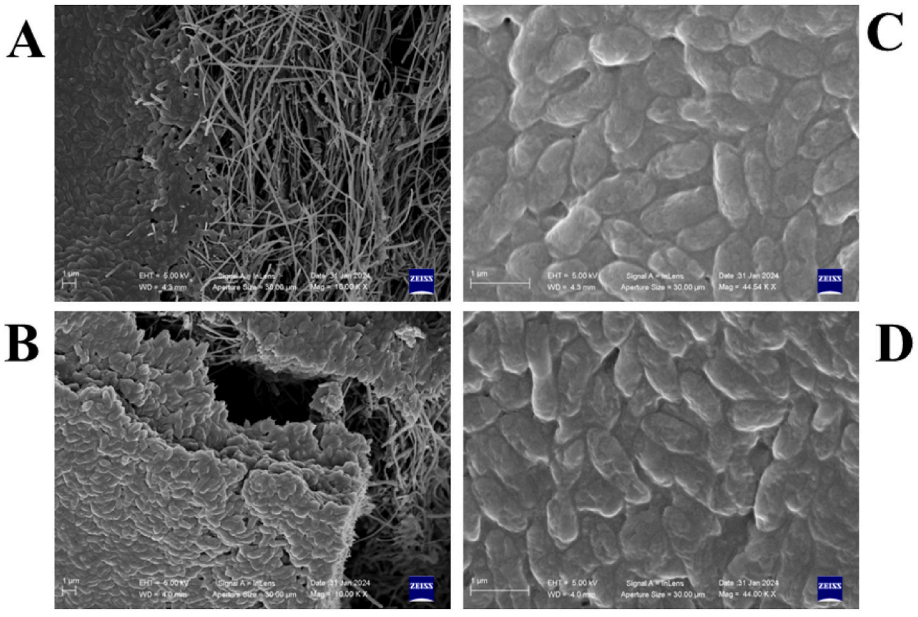

Fig. 1. SEM images of PHB-CF electrode with *R. capsulatus* cells in the PDA matrix not exposed (A) and exposed to $NiCl_2$ (B). High magnification of the same samples not exposed (C) and exposed to $NiCl_2$ (D).

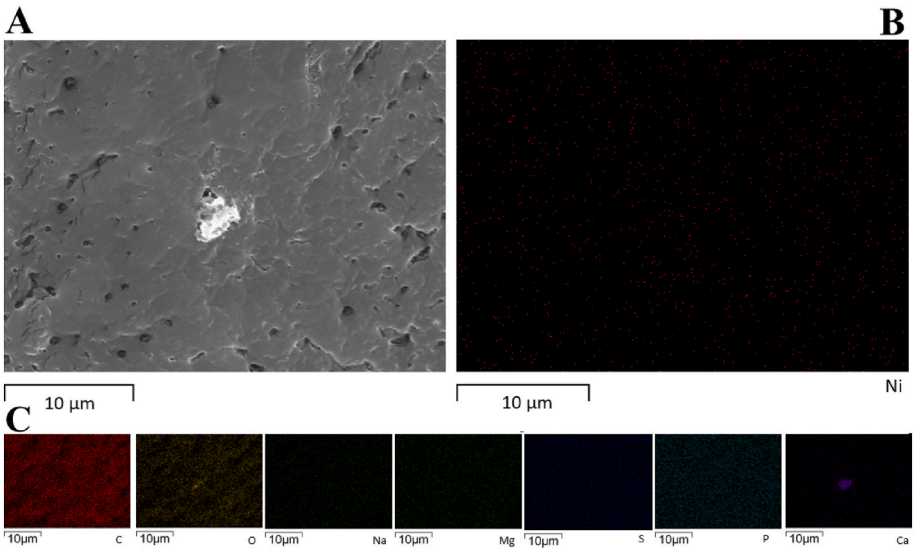

Fig. 2. SEM micrograph of PHB-CF electrode with *R. capsulatus* cells in the PDA matrix exposed to $NiCl_2$ (A), EDS mapping of $NiCl_2$ (B) and other atoms on the same electrode area (C).

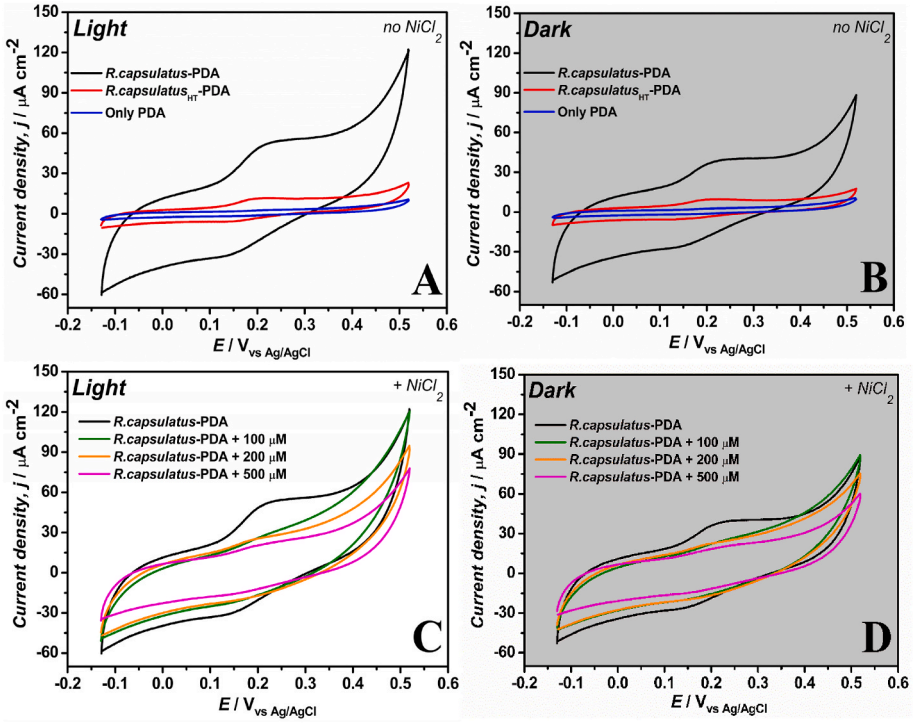

Fig. 3. CVs for the biophotoanode under light (A) and dark conditions (B), for *R.caps*-PDA (black line); heat-treated $R.caps_{HT}$-PDA (red line); and only PDA (blue line). The performance of the *R.caps*-PDA biohybrid photoanodes (black line) was evaluated with exposure to 100 µM (green line), 200 µM (orange line), and 500 µM (magenta line) $NiCl_2$ in the presence (C) and absence of light (D). CE: Pt; RE: Ag|AgCl (3 M NaCl). Scan rate = 5 mV s^{-1}; temperature = 25 °C.

presence of both metal ions at 100 µM and the CVs obtained for heat-treated microbial cells (Fig. 3 A) shows that the simultaneous presence of Ni and Cu ions resulted in the complete inhibition of the microbial activity. The same behavior was observed also in the dark, with a 40 % decrease in catalytic activity in the presence of both metal ions. Interestingly, the inhibitory effects of both metal ions could be better evidenced when studying the performance of the biophotoelectrodes under illumination, remarking on the relevance of utilizing photosynthetic organisms for the development of the biosensor. Based on these results, we further investigated photocurrent generation over time when the biophotoelectrodes are exposed to different concentrations of $NiCl_2$ and $CuSO_4$ (Fig. 4).

Fig. 4 A shows the profile of the amperometric curves acquired for the hybrid electrode that revealed an active system under illumination at 1000 s (22 ± 2 µA cm^{-2}), generating a 3-fold and 6-fold higher current density compared to the $R.caps_{HT}$-PDA and only PDA, respectively. Indeed, the *R.caps*-PDA catalyst electrode generated a total charge of 63 ± 4 mC, which was 3-fold and 7-fold higher than the total generated charge achieved with the $R.caps_{HT}$-PDA (22 ± 1 mC), and only PDA (9 ± 1 mC), respectively. This result further confirms the enhanced catalytic interaction between *R. capsulatus* and the electrode by the electropolymerized PDA, which improves the transfer of electrons to the

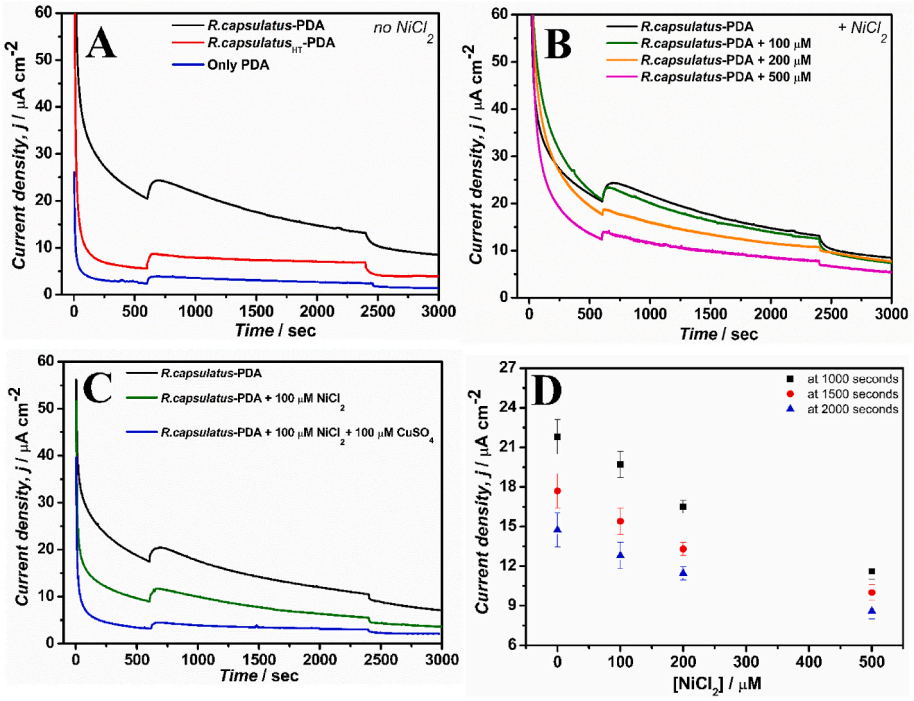

Fig. 4. Amperometric i-t traces at + 0.32 V for (A) *R.caps*-PDA (black line); heat-treated *R.caps*$_{HT}$-PDA (red line); and only PDA (blue line). (B) Performance of the *R.caps*-PDA biohybrid photoanodes (black line) after being exposed to 100 μM (green line), 200 μM (orange line), and 500 μM (magenta line) $NiCl_2$ in the presence and absence of light. (C) Performance of the *R.caps*-PDA biohybrid photoanodes (black line) exposed to only 100 μM $NiCl_2$ (green line) and 100 μM of $NiCl_2$ + $CuSO_4$ (blue line) in the presence and absence of light. D) Comparison of the current density generated vs different $NiCl_2$ concentrations at different timing: 1000 s (black square), 1500 s (red circle), and 2000 s (blue triangle). The experiments were performed in three steps: 600 s in the dark, 1800 s in the light, and 600 s in the dark. Experiment total time = 3000 s. CE: Pt; RE: Ag|AgCl (3 M NaCl).

electrode surface.

While the CV experiments revealed that the hybrid system achieved a high catalytic activity, we aimed to evaluate further the variation in current generation over time of the *R.caps*-PDA biophotoelectrode when exposed to $NiCl_2$ to develop the biosensor. As shown in Fig. 4 B, the biohybrid system (black line) showed a gradual decrease in current density for increasing concentrations of $NiCl_2$, eventually reaching a 40 % decrease after the addition of 500 μM $NiCl_2$ for 35 ± 2 mC of charge generated.

The *R.caps*-PDA electrode exposed to Ni^{2+} and Cu^{2+} (Fig. 4 C) under illumination at 1000 s achieved 4 ± 0.5 μA cm^{-2}, generating a 5-fold and 3-fold lower current density compared to the *R.caps*-PDA and *R. caps*-PDA + $NiCl_2$, respectively. The chronoamperometric measurements corroborate with the results obtained by CV, providing a sharp decrease in the catalytic activity when the hybrid system is exposed to more than one pollutant. These results underline the challenge of obtaining selective sensing systems utilizing intact metabolically active bacteria. However, promising results have been reported on the possibility of utilizing synthetic biology (Atkinson et al., 2022) or specific operating modes (Jiang et al., 2017) to achieve selectivity in bacteria-based biosensors.

We also conducted chronoamperometry experiments with *R.caps*$_{HT}$-PDA (Figure S6 A) and only PDA (Figure S6 B) in the presence and absence of $NiCl_2$ and no significant variation in current density was observed, which agrees with CV results (Figs. S3 and S4). On the other hand, the results with the control electrode containing only PDA confirmed that the current density profile is similar in the presence or absence of metal ions, due to the pollutants not affecting the abiotic photocurrent obtained.

Fig. 4 D highlights the correlation obtained between $NiCl_2$ concentration and current density obtained for the biohybrid systems at different sampling times. Interestingly, the best linear correlation is already obtained after 1000s, shortening the time required for metal ions monitoring. Based on the promising results obtained, future studies should focus on exploring the effects of different metal ions and their simultaneous presence in the electrolyte on photocurrent response.

3.2. Spectroscopic studies

Spectroscopic studies were performed to investigate if the exposure to $NiCl_2$ affected the stability of the photosynthetic apparatus in the bacterial cells. As shown in Figure S7 (A-D) the spectroscopy results did not show wide alteration in the photosynthetic apparatus of the bacterium, even with the addition of the pollutant, with no major shifts for the characteristic absorption peaks. Accordingly, it can be concluded that the exposure to different concentrations of $NiCl_2$ does not significantly affect the photosynthetic apparatus, and the loss in photocurrent obtained in CVs and chronoamperometry studies is not directly related to an inhibition of the photosynthetic apparatus but rather of the metabolic activity of the bacterial cells. These findings agree with the work of Torquato et al. (de Moura Torquato et al., 2023), where exposure of *R. capsulatus* cells entrapped in a PDA matrix to 300 μM 2,4-dinitrophenol did not significantly affect the photosynthetic apparatus.

3.3. Photoelectrochemical assessment of R. capsulatus-PDA in a complex matrix

Following the initial characterization of the biohybrid system in a simple electrolyte, we studied the performance of the hybrid system when operating in a complex electrolyte containing 10 % commercial beer with the addition of different concentrations of $NiCl_2$. Fig. 5 A shows the chronoamperometric assays for *R.caps*-PDA (black line), *R. caps*-PDA in the complex matrix (red line), and *R.caps*-PDA with the addition of different concentrations of $NiCl_2$, specifically 100 μM (green line), 200 μM (orange line), and 500 μM (magenta line). Fig. 5 B displays the relation between the current density achieved at 1000 s *vs* the

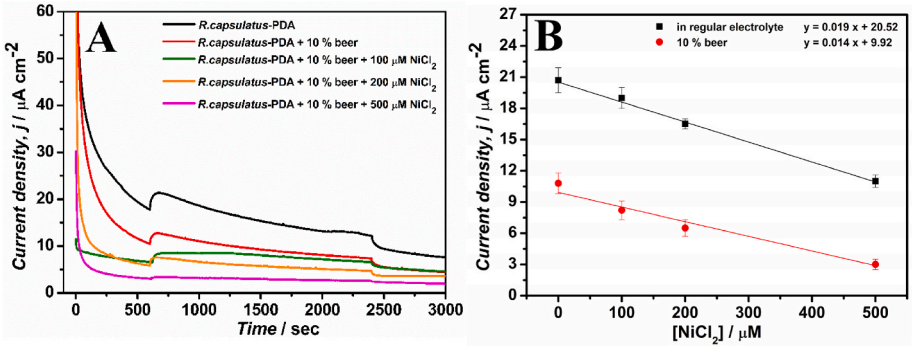

Fig. 5. A) Amperometric i-t traces at + 0.32 V for *R.caps*-PDA with 10 % beer exposed to 100 μM (green), 200 μM (orange), and 500 μM (magenta). B) Comparison of the current density generated at 1000 s for *R.caps*-PDA in regular electrolyte (black) and with the additon of 10% beer (v/v). The experiments were performed in three steps: 600 s in the dark, 1800 s in the light, and 600 s in the dark. Experiment total time = 3000 s. CE: Pt; RE: Ag|AgCl (3 M NaCl).

different configurations performed for *R.caps*-PDA, *R.caps*-PDA containing 10 % beer, and *R.caps*-PDA with 10 % beer and $NiCl_2$.

The amperometric profile for the hybrid system achieved, at 1000 s, a current density of 19 ± 1 μA cm^{-2}, while the bioelectrode containing 10 % beer showed a decreased response, reaching 11 ± 1 μA cm^{-2}, accounting for a 40 % decrease in catalytic activity when operating in the complex electrolyte. On the other hand, despite the decreased catalytic activity in the presence of beer, it is important to note that it was still possible to obtain a linear relation between the current density and the concentration of $NiCl_2$, with decreasing current densities of 8 ± 1 μA cm^{-2}, 7 ± 1 μA cm^{-2}, and 3 ± 1 μA cm^{-2} at 1000 s for 100, 200, and 500 μM $NiCl_2$, respectively. Therefore, the system containing 10 % beer and 500 μM of $NiCl_2$ showed a decrease of 80 % in photocurrent generated compared to the *R.caps*-PDA electrode (Fig. 5 A). The sensibility of the hybrid system based on [$NiCl_2$] *vs.* current density comparison shown in Fig. 5 B is 0.019 μA cm^{-2} L mol^{-1} operating in the regular electrolyte while in the complex matrix is 30 % lower (0.014 μA cm^{-2} L mol^{-1}). Therefore, while the biophotoanode in the regular electrolyte proved to be more sensitive, the biophotoelectrodeallowed a good linear correlation also in the system containing 10 % beer (R^2 = 0.99). Additionally, the low standard deviation confirms the good reproducibility of the approach. Table 1 highlights and compares the charge generated for all bioelectrodes analyzed in Figs. 4 and 5 during the amperometric tests.

The charge generated for the hybrid electrode operating in the complex electrolyte was 2-fold lower related to the *R.caps*-PDA, revealing a decrease in energy generation by the metabolic activity of the bacteria. Furthermore, it is important to note that all electrodes containing 10 % beer and $NiCl_2$ provided low charge values after 3000 s of polarization. The *R.caps*-PDA containing 10 % beer and 500 μM $NiCl_2$ reached only 9 ± 1 mC, achieving a final charge 4-fold, and 7-fold lower than *R.caps*-PDA +500 μM $NiCl_2$ and *R.caps*-PDA, respectively.

Fig. S8 shows the cyclic voltammetry experiments for *R.caps*-PDA (black line), *R.caps*-PDA in the complex electrolyte containing 10 % beer (red); and *R.caps*-PDA with 10 % beer + 100 μM (green), 200 μM (orange), and 500 μM (magenta) $NiCl_2$ in both light (A) and dark (B). The voltammetric responses obtained with the complex electrolyte in the absence and presence of contaminants corroborate the results presented in Fig. 5, which pave the way for implementing the biohybrid electrode in complex solutions.

Table 1
Evaluation of the charge generated during the amperometry tests for the *R. caps*-PDA bioelectrodes in the presence and absence of the real sample and addition of 100, 200, and 500 $NiCl_2$.

Charge generated (mC)		*R. caps*-PDA	*R.caps*-PDA + 100 μM $NiCl_2$	*R.caps*-PDA + 200 μM $NiCl_2$	*R.caps*-PDA + 500 μM $NiCl_2$
	Without beer	63 ± 4	55 ± 3	48 ± 2	35 ± 2
	With 10 % beer (real sample)	32 ± 3	21 ± 1	18 ± 1	9 ± 1

3.4. Self-powered operation

Power density tests were performed by coupling the developed biohybrid photoanode to a Pt cathode, to evaluate (i) if the system could produce power, operating as a photo-microbial fuel cell, and (ii) if the presence of $NiCl_2$ would affect the performance of the device, enabling operation as a self-powered biosensor. Fig. 6 A displays the power density tests for the *R.caps*-PDA (black line); heat-treated *R.caps*$_{HT}$-PDA (red line); and only PDA (blue line) electrodes, while Fig. 6 B shows the influence of 500 μM of $NiCl_2$ on the power density.

The maximum current and power densities of the *R.caps*-PDA (black line) were 4.2 ± 0.3 μA cm^{-2} and 0.46 ± 0.04 μW cm^{-2}, respectively. While the *R.caps*$_{HT}$-PDA (red line) achieved a maximum current and power densities of only 1.6 ± 0.1 μA cm^{-2} and 0.12 ± 0.02 μW cm^{-2}, respectively. Also, for the control cell obtained using as anode the abiotic electrode modified only with PDA the power density was 0.10 ± 0.03 μW cm^{-2}. Remarkably, the biohybrid anode achieved a power density 4-fold higher than the cell operating with the control anodes *R. caps*$_{HT}$-PDA and only PDA.

It is interesting to underline that the power density profile for the two-electrode self-powered system with the photosynthetic hybrid bioanode demonstrated a decrease in catalytic activity as the metal concentration was increased (Fig. 6 B). Specifically, in the presence of 100 μM and 200 μM $NiCl_2$, power densities of 0.26 ± 0.02 μW cm^{-2} and 0.17 ± 0.01 μW cm^{-2} were observed, respectively. Consequently, the energy output of the self-powered microbial electrochemical sensors was reduced by 45 % and 55 % when exposed to 100 μM and 200 μM of contaminant, respectively. When increasing the concentration of the contaminant to 500 μM $NiCl_2$ (Fig. 6 B, magenta), the photo-microbial fuel cell with *R.caps*-PDA as anode provided maximum current and power densities of 1.3 ± 0.3 μA cm^{-2} and 0.10 ± 0.01 μW cm^{-2}, respectively, corresponding to an 80 % decrease compared with the operation of the device in the absence of $NiCl_2$. It should be underlined that while the power production of the photo-microbial fuel cells is relatively low, it allowed self-power operation of the biosensor and correlation of the power density with metal ions concentration. Future studies should be focused on further improving power output performance, exploring different device geometries and electrode materials (Saar et al., 2018), which could pave the way to the use of the biohybrid system for localized power production coupled with environmental monitoring.

Figures S9 A and S9 B show the control-fuel cells with *R.caps*$_{HT}$-PDA

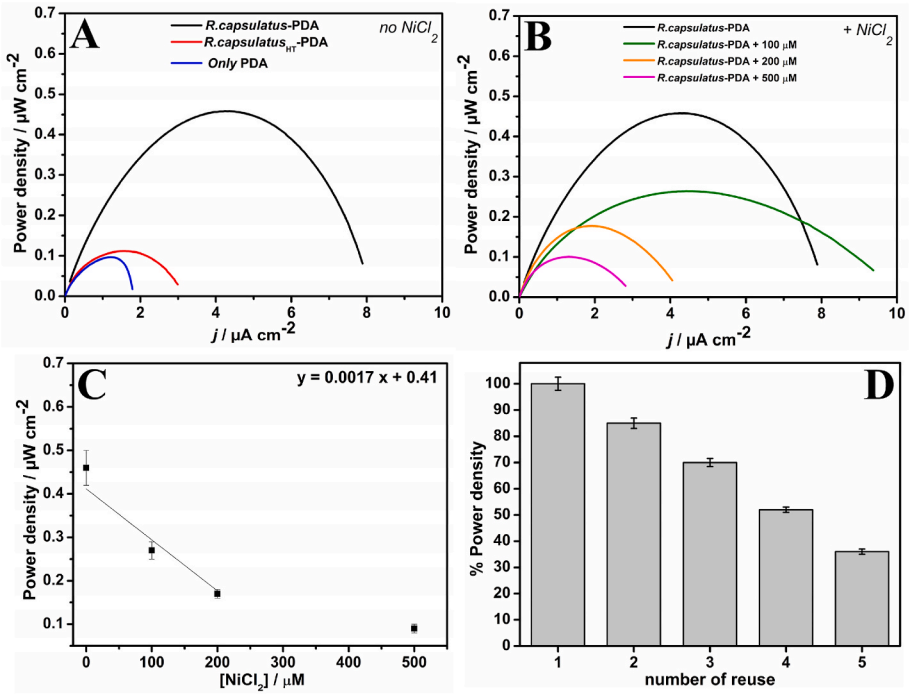

Fig. 6. A) Power density curves performed under illumination for *R.caps*-PDA (black line); heat-treated *R.caps*$_{HT}$-PDA (red line); and only PDA (blue line). B) Performance of the complete photo-microbial fuel cell with *R.caps*-PDA photoanodes in the presence of 100 (green), 200 (orange), and 500 (magenta) µM $NiCl_2$. C) Calibration plot of the self-powered system for the power density generated in the absence of $NiCl_2$ compared to the system exposed to 100 µM, 200 µM, and 500 µM $NiCl_2$. D) Comparison of the power density percentage over the number of reuses of the complete photo-microbial fuel cell with *R.caps*-PDA photoanodes after successive applications.

and only PDA anodes in the absence (black line) and presence (red line) of 500 µM of $NiCl_2$. The results of both control-fuel cells achieved similar power density values, showing that the presence of metabolically active bacteria is needed to monitor the contaminant. A further control was performed by adding in the complete photo-microbial fuel cells a volume of only MOPS buffer (without $NiCl_2$) equal to the one used for $NiCl_2$ addition. The results presented in Fig. S10 confirmed that the addition of electrolyte without metal ions does not interfere with the device's power generation.

The power density results for the photo-microbial fuel cell exposed to different metal-ions concentrations unveiled an inverse correlation between power density and $NiCl_2$ concentration (Fig. 6 C). Interestingly, a linear correlation could be obtained up to 200 µM $NiCl_2$. Increasing the metal-ions concentrations to 500 µM resulted in the apparent complete loss of biocatalytic activity (power density similar to the one obtained with dead bacteria and in the absence of bacteria, Fig. 6 A) with the power density output no longer linearly correlated to the metal-ions concentration. Accordingly, the results underline that a preliminary correlation between power density and $NiCl_2$ can be performed for low concentrations in the range 0–200 µM, while an on/off type of response of the self-powered system is obtained in the presence of higher concentrations of the contaminant.

Furthermore, the possibility of reusing the photo-microbial fuel cell as self-powered biosensors for multiple analyses was assessed by repeating sequential power density analyses (Fig. 6 D). After three reuse cycles, the system maintained 70 % of its original maximum power density. This value allows for the use of the self-powered system for $NiCl_2$ monitoring paving the way to the promising possibility of performing the early monitoring of metal ion contaminants via rapid analysis. Additional reuses caused a drop in maximum power density (52 and 36 % of the maximum power output for four and five reuses, respectively), which would not allow a proper application of the biosensor. It is important to remark that the reuse was tested without exposing the bacteria to the contaminant.

Table 2 compares the photocurrent production obtained in the present work with studies published in the last years employing a photo-bioelectrocatalytic system containing intact photosynthetic bacteria, underlining the increasing research interest in photosynthetic bacteria-modified electrode. Notably, our biophotoelectrode significantly improved the photocurrent generated compared with the previous studies. Thereby, the enhanced biohybrid system opens opportunities for the future application of intact photosynthetic bacteria-based photobioelectrochemical systems for biosensing and remediation platforms in wastewater.

4. Conclusion

We have shown that hybrid biophotoelectrodes obtained on a bio-based PHB-CF electrode modified with a PDA-*Rhodobacter capsulatus* matrix allowed studying the effects of metal ions contaminants on purple bacteria photobioelectrocatalysis, unveiling a linear relation between current density generation and Ni^{2+} in the range 100–500 µM when operating in a three-electrode system. The obtained biohybrid photoanodes could also operate in a complex electrolyte while maintaining a linear relation between Ni^{2+} and current density generation. Finally, the implementation of the biophotoelectrode in a complete single-chamber photo-microbial fuel cell resulted in a power output affected by the presence of $NiCl_2$ in the electrolyte, paving the way for the future development of low-cost, on-demand, self-powered biosensors performing in-situ monitoring of pollutants in the water environment with no need for trained personnel.

CRediT authorship contribution statement

Jefferson Honorio Franco: Writing – original draft, Methodology, Investigation, Formal analysis, Data curation. **Paolo Stufano:** Methodology. **Rossella Labarile:** Formal analysis, Data curation. **Dario Lacalamita:** Validation, Formal analysis. **Pierluigi Lasala:** Formal analysis.

Table 2
Comparison of photocurrent density for different electrode configurations based on photosynthetic bacteria.

Highlights	Photosynthetic organisms	Photocurrent density	Applied potential	Self-powered biosensor operation	Reference
Photosynthetic bacteria-based electrodes for self-powered metal ions monitoring	Purple non-sulfur bacterium *Rhodobacter capsulatus*	+58 ± 3 μA cm^{-2} (value from cyclic voltammetry)	+0.32 V *vs.* Ag|AgCl	yes	Our work
Microbial fuel cell with purple bactéria	*Rhodopseudomonas palustris* DX-1	~ +30 μA cm^{-2} (value from cyclic voltammetry with carbon paper electrodes)	+0.0 V *vs.* Ag|AgCl	no	(Xing et al., 2008)
Cyanobacteria-based biosensor with redox mediator	Cyanobacterium *Anabaena variabilis*	~30 μA cm^{-2} with diffusible mediator; 9 ± 3 μA cm^{-2} with immobilized redox mediator	+0.5 V *vs.* SCE	no	(Tucci et al., 2019b)
Cyanobacteria-based biosensor with direct electron transfer	Cyanobacterium *Synechocystis* PCC6803	0.7 μA	+0.4 V *vs.* Ag|AgCl	no	(Tucci et al., 2019a)
Determination of rate determining step in purple bacteria PEET	Purple non-sulfur bacterium *Rhodobacter capsulatus*	2.9 ± 0.5 μA cm^{-2}	+0.36 V *vs.* SCE	no	(Grattieri et al., 2019)
Electrochemical characterization of metal nanoprecipitates by *Rhodobacter capsulatus*	Purple non-sulfur bacterium *Rhodobacter capsulatus*	17 ± 0.2 μA cm^{-2}	+0.10 V *vs.* Ag|AgCl	no	(Borghese et al., 2020)
Elucidation of salinity effects on biophotoelectrocatalysis	Purple non-sulfur bacterium *Rhodobacter capsulatus*	3.4 ± 0.2 μA cm^{-2}	+0.36 V *vs.* SCE	no	(Gaffney et al., 2020)
Quinone-based redox polymer for PEET and decreased inhibition	Purple non-sulfur bacterium *Rhodobacter capsulatus*	2.7 ± 0.9 μA cm^{-2}	+0.073 V *vs.* SCE	no	(Grattieri et al., 2020b)
Determination of substrate modulation effects on photobioelectrocatalysis	Purple non-sulfur bacterium *Rhodobacter capsulatus*	10 ± 2 μA cm^{-2}	+0.36 V *vs.* SCE	no	(Beaver et al., 2022)
Bio-Inspired Redox-Adhesive Polydopamine Matrix for Intact Bacteria Biohybrid Photoanodes	Purple non-sulfur bacterium *Rhodobacter capsulatus*	+0.94 ± 0.05 μA cm^{-2}	+0.32 V *vs.* Ag|AgCl	no	(Buscemi et al., 2022)
Photobioelectrocatalysis of Photosynthetic Bacteria Exposed to Dinitrophenol	Purple non-sulfur bacterium *Rhodobacter capsulatus*	+1.02 ± 0.28 μA cm^{-2} (value from cyclic voltammetry)	+0.32 V *vs.* Ag|AgCl	no	(de Moura Torquato et al., 2023)
Bacterial- polyhydroxybutyrate for Biocompatible Microbial Electrodes	Purple non-sulfur bacterium *Rhodobacter capsulatus*	+48 ± 10 μA cm^{-2} (value from cyclic voltammetry)	+0.32 V *vs.* Ag|AgCl	no	(de Moura Torquato et al., 2024)
In vivo polydopamine coating of *Rhodobacter sphaeroides* for enhanced electron transfer	Purple non-sulfur bacterium *Rhodobacter sphaeroides*	+8.56 ± 0.13 μA cm^{-2}	+0.23 V *vs.* Ag|AgCl	no	(Labarile et al., 2024)

Elisabetta Fanizza: Supervision, Funding acquisition. **Massimo Trotta:** Supervision, Funding acquisition. **Gianluca Maria Farinola:** Supervision, Funding acquisition. **Matteo Grattieri:** Writing – review & editing, Supervision, Funding acquisition, Conceptualization.

Declaration of competing interest

The authors declare that they have no known competing financial interests or personal relationships that could have appeared to influence the work reported in this paper.

Acknowledgments

Matteo Grattieri and Jefferson H. Franco would like to acknowledge the funding from Fondazione CON IL SUD, Grant, project number 2018-PDR-00914. R. Labarile and M. Trotta acknowledges funding from Fonds National Suisse de la Recherche Scientifique, project Phosbury-Photosynthetic bacteria in Self-assembled Biocompatible coatings for the transduction of energy (Project Nr CRSII5_205925/1). M. Trotta acknowledges the project PrinPNRR2022—P20225NFS4 (PhOLcs—-Photosynthesis for Organic Light-Powered Electronics). D. Lacalamita would like to thank ENI SPA for the PhD fellowship “Da acque reflue a H_2 per bioelettrolisi microbica”.

Appendix A. Supplementary data

Supplementary data to this article can be found online at https://doi.org/10.1016/j.biosx.2024.100552.

Data availability

Data will be made available on request.

References

Ahmad, F., Khan, M.A., Waqas, U., Ramay, S.M., Atiq, S., 2023a. Elucidating an efficient super-capacitive response of a Sr2Ni2O5/rGO composite as an electrode material in supercapacitors. RSC Adv. 13, 25316–25326. https://doi.org/10.1039/D3RA03140C.

Ahmad, F., Shahzad, A., Danish, M., Fatima, M., Adnan, M., Atiq, S., Asim, M., Khan, M. A., Ain, Q.U., Perveen, R., 2024. Recent developments in transition metal oxide-based electrode composites for supercapacitor applications. J. Energy Storage 81, 110430. https://doi.org/10.1016/j.est.2024.110430.

Ahmad, F., Zahid, M., Jamil, H., Khan, M.A., Atiq, S., Bibi, M., Shahbaz, K., Adnan, M., Danish, M., Rasheed, F., Tahseen, H., Shabbir, M.J., Bilal, M., Samreen, A., 2023b. Advances in graphene-based electrode materials for high-performance supercapacitors: a review. J. Energy Storage 72, 108731. https://doi.org/10.1016/j.est.2023.108731.

Alfieri, M., Panzella, L., Oscurato, S., Salvatore, M., Avolio, R., Errico, M., Maddalena, P., Napolitano, A., d'Ischia, M., 2018. The chemistry of polydopamine film formation: the amine-quinone interplay. Biomimetics 3, 26. https://doi.org/10.3390/biomimetics3030026.

Anchidin-Norocel, L., Savage, W.K., Gutt, G., Amariei, S., 2021. Development, optimization, characterization, and application of electrochemical biosensors for detecting nickel ions in food. Biosensors 11. https://doi.org/10.3390/bios11120519.

Atkinson, J.T., Su, L., Zhang, X., Bennett, G.N., Silberg, J.J., Ajo-Franklin, C.M., 2022. Real-time bioelectronic sensing of environmental contaminants. Nature 611, 548–553. https://doi.org/10.1038/s41586-022-05356-y.

Beaver, K., Dantanarayana, A., Zani, A.B., Lehto, D.L., Minteer, S.D., 2023. Nitric oxide as a signaling molecule for biofilm formation and dispersal in mediated electron transfer microbial electrochemical systems. J. Electrochem. Soc. 170, 045503. https://doi.org/10.1149/1945-7111/acc97e.

Beaver, K., Gaffney, E.M., Minteer, S.D., 2022. Understanding metabolic bioelectrocatalysis of the purple bacterium Rhodobacter capsulatus through substrate modulation. Electrochim. Acta 416, 140291. https://doi.org/10.1016/j.electacta.2022.140291.

Bedendi, G., De Moura Torquato, L.D., Webb, S., Cadoux, C., Kulkarni, A., Sahin, S., Maroni, P., Milton, R.D., Grattieri, M., 2022. Enzymatic and Microbial Electrochemistry: Approaches and Methods. ACS Meas. Sci. Au 2, 517–541. https://doi.org/10.1021/acsmeasuresciau.2c00042.

Borghese, R., Malferrari, M., Brucale, M., Ortolani, L., Franchini, M., Rapino, S., Borsetti, F., Zannoni, D., 2020. Structural and electrochemical characterization of lawsone-dependent production of tellurium-metal nanoprecipitates by photosynthetic cells of Rhodobacter capsulatus. Bioelectrochemistry 133, 107456. https://doi.org/10.1016/j.bioelechem.2020.107456.

Buscemi, G., Vona, D., Stufano, P., Labarile, R., Cosma, P., Agostiano, A., Trotta, M., Farinola, G., Grattieri, M., 2022. Bio-Inspired redox-adhesive polydopamine matrix for intact bacteria biohybrid photoanodes. ACS Appl. Mater. Interfaces 14. https://doi.org/10.1021/acsami.2c02410.

Cui, Y., Lai, B., Tang, X., 2019. Microbial fuel cell-based biosensors. Biosensors 9. https://doi.org/10.3390/bios9030092.

Dai, Z., Xu, Z., Wang, T., Fan, Y., Liu, Y., Yu, R., Zhu, G., Lu, X., Li, B., 2019. In-situ oil presence sensor using simple-structured upward open-channel microbial fuel cell (UOC-MFC). Biosens. Bioelectron. X 1, 100014. https://doi.org/10.1016/j.biosx.2019.100014.

Das, K.K., Reddy, R.C., Bagoji, I.B., Das, S., Bagali, S., Mullur, L., Khodnapur, J.P., Biradar, M.S., 2019. Primary concept of nickel toxicity – an overview. J. Basic Clin. Physiol. Pharmacol. 30, 141–152. https://doi.org/10.1515/jbcpp-2017-0171.

de Moura Torquato, L.D., Lacalamita, D., Matteucci, R.M., Franco, J.H., Labarile, R., Perrotta, A., Trotta, M., Farinola, G.M., Boldrin Zanoni, M.V., Grattieri, M., Stufano, P., 2024. Bacterial-polyhydroxybutyrate for biocompatible microbial electrodes. J. Electrochem. Soc. 171, 055502. https://doi.org/10.1149/1945-7111/ad40d6.

de Moura Torquato, L.D., Matteucci, R.M., Stufano, P., Vona, D., Farinola, G.M., Trotta, M., Boldrin Zanoni, M.V., Grattieri, M., 2023. Photobioelectrocatalysis of intact photosynthetic bacteria exposed to dinitrophenol. Chemelectrochem 10, e202300013. https://doi.org/10.1002/celc.202300013.

Ding, Y.H., Floren, M., Tan, W., 2016. Mussel-inspired polydopamine for bio-surface functionalization. Biosurf Biotribol 2, 121–136. https://doi.org/10.1016/j.bsbt.2016.11.001.

ElMekawy, A., Hegab, H.M., Pant, D., Saint, C.P., 2018. Bio-analytical applications of microbial fuel cell–based biosensors for onsite water quality monitoring. J. Appl. Microbiol. 124, 302–313. https://doi.org/10.1111/jam.13631.

Fan, G., Wasuwanich, P., Furst, A.L., 2021. Biohybrid systems for improved bioinspired, energy-relevant catalysis. Chembiochem 22, 2353–2367. https://doi.org/10.1002/cbic.202100037.

Gaffney, E.M., Grattieri, M., Beaver, K., Pham, J., McCartney, C., Minteer, S.D., 2020. Unveiling salinity effects on photo-bioelectrocatalysis through combination of bioinformatics and electrochemistry. Electrochim. Acta 337, 135731. https://doi.org/10.1016/j.electacta.2020.135731.

Genchi, G., Carocci, A., Lauria, G., Sinicropi, M.S., Catalano, A., 2020. Nickel: human health and environmental toxicology. Int. J. Environ. Res. Publ. Health 17. https://doi.org/10.3390/ijerph17030679.

Giraud, E., Verméglio, A., 2008. Bacteriophytochromes in anoxygenic photosynthetic bacteria. Photosynth. Res. 97, 141–153. https://doi.org/10.1007/s11120-008-9323-0.

Grattieri, M., 2020. Purple bacteria photo-bioelectrochemistry: enthralling challenges and opportunities. Photochem. Photobiol. Sci. 19, 424–435. https://doi.org/10.1039/c9pp00470j.

Grattieri, M., Beaver, K., Gaffney, E.M., Dong, F., Minteer, S.D., 2020a. Advancing the fundamental understanding and practical applications of photo-bioelectrocatalysis. Chem. Commun. 56, 8553–8568. https://doi.org/10.1039/D0CC02672G.

Grattieri, M., Chen, H., Minteer, S.D., 2020. Chloroplast biosolar cell and self-powered herbicide monitoring. Chem. Commun. 56, 13161. https://doi.org/10.1039/d0cc03787g.

Grattieri, M., Minteer, S.D., 2018. Self-powered biosensors. ACS Sens. 3, 44–53. https://doi.org/10.1021/acssensors.7b00818.

Grattieri, M., Patterson, S., Copeland, J., Klunder, K., Minteer, S.D., 2020b. Purple bacteria and 3D redox hydrogels for bioinspired photo-bioelectrocatalysis. ChemSusChem 13, 230–237. https://doi.org/10.1002/cssc.201902116.

Grattieri, M., Rhodes, Z., Hickey, D.P., Beaver, K., Minteer, S.D., 2019. Understanding biophotocurrent generation in photosynthetic purple bacteria. ACS Catal. 9, 867–873. https://doi.org/10.1021/acscatal.8b04464.

Hasan, K., Bekir Yildiz, H., Sperling, E., Ó Conghaile, P., Packer, M.A., Leech, D., Hägerhäll, C., Gorton, L., 2014. Photo-electrochemical communication between cyanobacteria (Leptolyngbia sp.) and osmium redox polymer modified electrodes. Phys. Chem. Chem. Phys. 16, 24676–24680. https://doi.org/10.1039/C4CP04307C.

Hemdan, B., Garlapati, V.K., Sharma, S., Bhadra, S., Maddirala, S., K.M, V., Motru, V., Goswami, P., Sevda, S., Aminabhavi, T.M., 2022. Bioelectrochemical systems-based metal recovery: resource, conservation and recycling of metallic industrial effluents. Environ. Res. 204, 112346. https://doi.org/10.1016/j.envres.2021.112346.

Jiang, Y., Liang, P., Liu, P., Miao, B., Bian, Y., Zhang, H., Huang, X., 2017. Enhancement of the sensitivity of a microbial fuel cell sensor by transient-state operation. Environ. Sci.: Water Res. Technol. 3, 472–479. https://doi.org/10.1039/C6EW00346J.

Kamali, M., Guo, Y., Aminabhavi, T.M., Abbassi, R., Dewil, R., Appels, L., 2023. Pathway towards the commercialization of sustainable microbial fuel cell-based wastewater treatment technologies. Renew. Sustain. Energy Rev. 173, 113095. https://doi.org/10.1016/j.rser.2022.113095.

Kondaveeti, S., Govindarajan, D., Mohanakrishna, G., Thatikayala, D., Abu-Reesh, I.M., Min, B., Nambi, I.M., Al-Raoush, R.I., Aminabhavi, T.M., 2023. Sustainable bioelectrochemical systems for bioenergy generation via waste treatment from petroleum industries. Fuel 331, 125632. https://doi.org/10.1016/j.fuel.2022.125632.

Kumar, A., Hsu, L.H.-H., Kavanagh, P., Barrière, F., Lens, P.N.L., Lapinsonnière, L., Lienhard V, J.H., Schröder, U., Jiang, X., Leech, D., 2017. The ins and outs of microorganism–electrode electron transfer reactions. Nat. Rev. Chem 1, 24. https://doi.org/10.1038/s41570-017-0024.

Labarile, R., Vona, D., Varsalona, M., Grattieri, M., Reggente, M., Comparelli, R., Farinola, G.M., Fischer, F., Boghossian, A.A., Trotta, M., 2024. In vivo polydopamine coating of Rhodobacter sphaeroides for enhanced electron transfer. Nano Res. 17, 875–881.

Liu, S.-R., Cai, L.-F., Wang, L.-Y., Yi, X.-F., Peng, Y.-J., He, N., Wu, X., Wang, Y.-P., 2019. Polydopamine coating on individual cells for enhanced extracellular electron transfer. Chem. Commun. 55, 10535–10538. https://doi.org/10.1039/C9CC03847G.

Longatte, G., Sayegh, A., Delacotte, J., Rappaport, F., Wollman, F.-A., Guille-Collignon, M., Lemaître, F., 2018. Investigation of photocurrents resulting from a living unicellular algae suspension with quinones over time. Chem. Sci. 9, 8271–8281. https://doi.org/10.1039/C8SC03058H.

Niu, H., Zhang, J., Xie, Z., Wang, X., Lin, T., 2011. Preparation, structure and supercapacitance of bonded carbon nanofiber electrode materials. Carbon N Y 49, 2380–2388. https://doi.org/10.1016/j.carbon.2011.02.005.

Nurak, T., Praphairaksit, N., Chailapakul, O., 2013. Fabrication of paper-based devices by lacquer spraying method for the determination of nickel (II) ion in waste water. Talanta 114, 291–296. https://doi.org/10.1016/j.talanta.2013.05.037.

Operamolla, A., Ragni, R., Milano, F., Roberto Tangorra, R., Antonucci, A., Agostiano, A., Trotta, M., Farinola, G., 2015. "Garnishing" the photosynthetic bacterial reaction center for bioelectronics. J. Mater. Chem. C 3, 6471–6478. https://doi.org/10.1039/C5TC00775E.

Pankratova, G., Gorton, L., 2017. Electrochemical communication between living cells and conductive surfaces. Curr. Opin. Electrochem. 5, 193–202. https://doi.org/10.1016/j.coelec.2017.09.013.

Prévoteau, A., Rabaey, K., 2017. Electroactive biofilms for sensing: reflections and perspectives. ACS Sens. 2, 1072–1085. https://doi.org/10.1021/acssensors.7b00418.

Rezaei, B., Rezaei, E., 2006. Simultaneous determination of trace amounts of nickel, cobalt, and zinc in the wastewater of a galvanic workshop by using adsorptive cathodic stripping voltammetry. J. Anal. Chem. 61, 262–265. https://doi.org/10.1134/S1061934806030129.

Saar, K.L., Bombelli, P., Lea-Smith, D.J., Call, T., Aro, E.-M., Müller, T., Howe, C.J., Knowles, T.P.J., 2018. Enhancing power density of biophotovoltaics by decoupling storage and power delivery. Nat. Energy 3, 75–81. https://doi.org/10.1038/s41560-017-0073-0.

Santoro, C., Arbizzani, C., Erable, B., Ieropoulos, I., 2017. Microbial fuel cells: from fundamentals to applications. A review. J. Power Sources 356, 225–244. https://doi.org/10.1016/j.jpowsour.2017.03.109.

Sayegh, A., Perego, L.A., Arderiu Romero, M., Escudero, L., Delacotte, J., Guille-Collignon, M., Grimaud, L., Bailleul, B., Lemaître, F., 2021. Finding adapted quinones for harvesting electrons from photosynthetic algae suspensions. Chemelectrochem 8, 2968–2978. https://doi.org/10.1002/celc.202100757.

Simoska, O., Gaffney, E.M., Minteer, S.D., Franzetti, A., Cristiani, P., Grattieri, M., Santoro, C., 2021. Recent Trends and Advances in Microbial Electrochemical Sensing Technologies: An Overview. Curr. Opin. Electrochem. 30, 100762. https://doi.org/10.1016/j.coelec.2021.100762.

Tibazarwa, C., Corbisier, P., Mench, M., Bossus, A., Solda, P., Mergeay, M., Wyns, L., van der Lelie, D., 2001. A microbial biosensor to predict bioavailable nickel in soil and its transfer to plants. Environ. Pollut. 113, 19–26. https://doi.org/10.1016/S0269-7491(00)00177-9.

Torquato, L.D. de M., Grattieri, M., 2022. Photobioelectrochemistry of intact photosynthetic bacteria: advances and future outlook. Curr. Opin. Electrochem. 34, 101018. https://doi.org/10.1016/j.coelec.2022.101018.

Tucci, M., Bombelli, P., Howe, C.J., Vignolini, S., Bocchi, S., Schievano, A., 2019a. A storable mediatorless electrochemical biosensor for herbicide detection. Microorganisms 7. https://doi.org/10.3390/microorganisms7120630.

Tucci, M., Grattieri, M., Schievano, A., Cristiani, P., Minteer, S.D., 2019b. Microbial amperometric biosensor for online herbicide detection: photocurrent inhibition of Anabaena variabilis. Electrochim. Acta 302, 102–108. https://doi.org/10.1016/j.electacta.2019.02.007.

Verma, N., Singh, M., 2006. A Bacillus sphaericus based biosensor for monitoring nickel ions in industrial effluents and foods. J. Autom. Methods Manag. Chem., 83427 https://doi.org/10.1155/JAMMC/2006/83427, 2006.

Xing, D., Zuo, Y., Cheng, S., Regan, J.M., Logan, B.E., 2008. Electricity generation by rhodopseudomonas palustris DX-1. Environ. Sci. Technol. 42, 4146–4151. https://doi.org/10.1021/es800312v.

Yadav, D., Amini, F., Ehrmann, A., 2020. Recent advances in carbon nanofibers and their applications – a review. Eur. Polym. J. 138, 109963. https://doi.org/10.1016/j.eurpolymj.2020.109963.

Yu, D., Bai, L., Zhai, J., Wang, Y., Dong, S., 2017. Toxicity detection in water containing heavy metal ions with a self-powered microbial fuel cell-based biosensor. Talanta 168, 210–216. https://doi.org/10.1016/j.talanta.2017.03.048.

Yun, J., Kim, T., Hong, H., Kim, Y.J., Kim, S. Il, Park, Y., Kim, K., Ryu, W., 2022. Conductive thylakoid composites with mussel-adhesive protein-coated carbon nanotubes for harvesting photosynthetic electrons. Appl. Surf. Sci. 575, 151697. https://doi.org/10.1016/j.apsusc.2021.151697.

Zdrojewicz, Z., Popowicz, E., Winiarski, J., 2016. [Nickel - role in human organism and toxic effects]. Pol. Merkur. Lek. 41, 115–118.

Zhang, T., Tremblay, P.-L., 2017. Hybrid photosynthesis-powering biocatalysts with solar energy captured by inorganic devices. Biotechnol. Biofuels 10, 249. https://doi.org/10.1186/s13068-017-0943-5.

Zhu, H., Wang, H., Zhang, Y., Li, Y., 2023. Biophotovoltaics: recent advances and perspectives. Biotechnol. Adv. 64, 108101. https://doi.org/10.1016/j.biotechadv.2023.108101.